Volume 6 · No. 9 – May 7 2010

D15063

NANO MICRO

small

www.small-journal.com

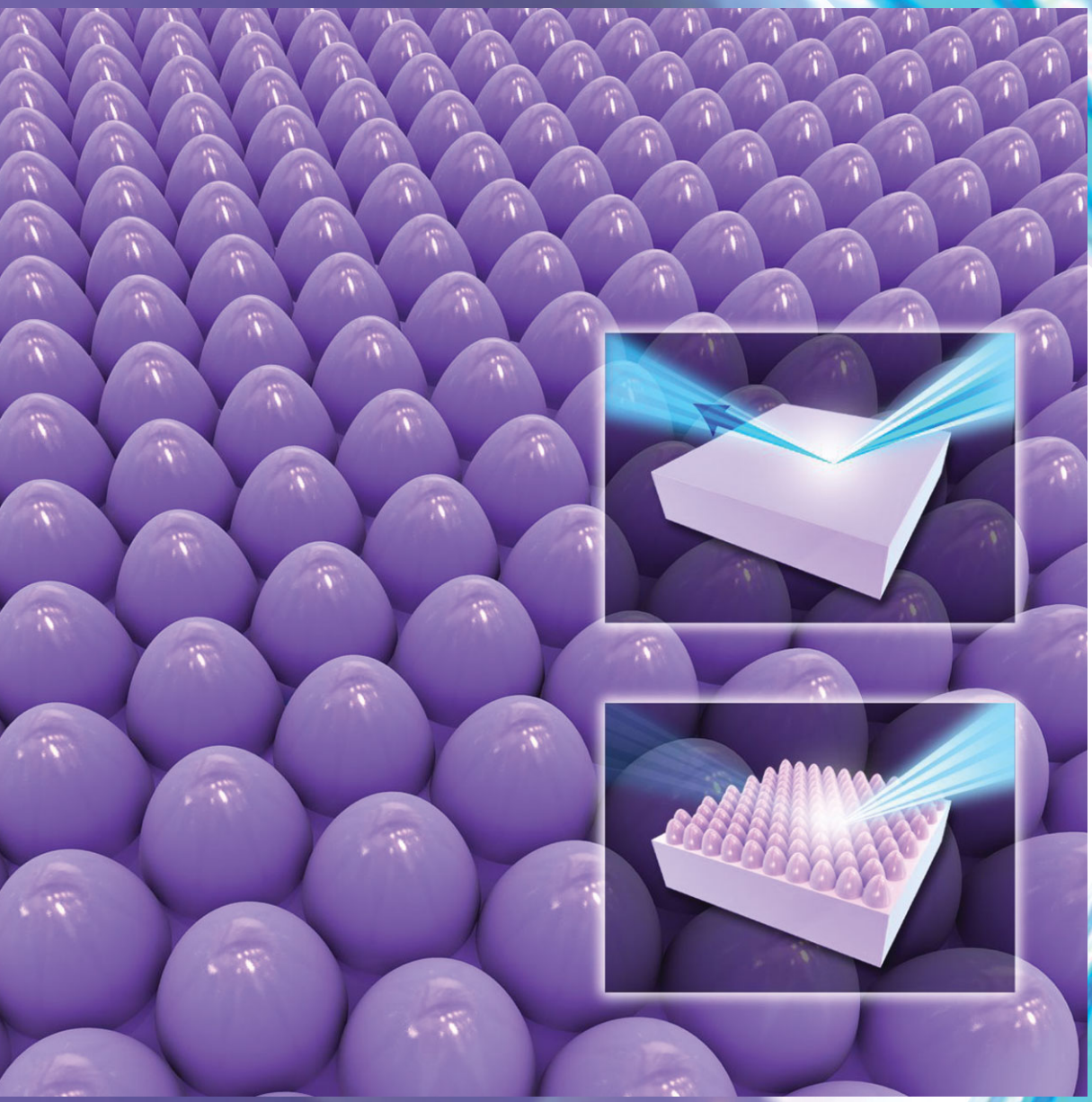

9/2010

WILEY-VCH

Bioinspired Parabola Subwavelength Structures for Improved Broadband Antireflection

Y. T. Lee et al.

Biomimetics

Bioinspired Parabola Subwavelength Structures for Improved Broadband Antireflection**

*Young Min Song, Sung Jun Jang, Jae Su Yu, and Yong Tak Lee**

Recently, there has been growing interest in the fabrication and study of broadband antireflective nanostructures for new technology applications in various fields, such as photovoltaic devices, light-emitting diodes, light sensors, and transparent glasses.[1–9] Over the past decade, many different structures, including gratings,[3,8,10–14] pyramids,[15] porous structures,[4,5,16] nanorods/nanocones,[17–26] and nanotips,[7,27–29] have been reported for antireflection purposes. To suppress the Fresnel reflection at the interface between air and a substrate material, tapered structures are required with dimension smaller than the optical wavelength. Moreover, a taller height with high packing density is desirable to enhance the antireflection properties in the broadband wavelength range.[14] From this point of view, nanotip arrays with a tip height up to 1 μm, which have been successfully fabricated using a self-mask etch or colloidal crystal etch process by several research groups,[28,29] are ideal for broadband antireflection use. In practical device applications (e.g., solar cells), however, it is evident that a taller height imposes a heavy burden on the fabrication procedure upon considering the epitaxial layer structure. Hence, it is crucial to determine an optimum geometry of subwavelength structures (SWSs) in a given height.

By the observation of corneal nipple arrays of various butterfly species and reflectance calculations of three different types of SWSs using a thin-film multilayer model, Stavenga et al. showed that the parabola shape provides better antireflection properties than cone and Gaussian-bell shapes.[30] In effective medium theory, the parabola shape yields a nearly linear refractive index gradient, which is efficient to reduce the surface reflection. To obtain SWSs with a conical profile, many fabrication methods, such as electron-beam/interference lithography,[3,8,10–14] nanoimprint lithography,[12,17,18] nanosphere or colloid formation,[15,19–21] metal nanoparticles,[22,23] and Langmuir–Blodgett assembly,[25,26] have been proposed. However, it is difficult for these techniques to guarantee the formation of the parabola shape because the shape of the SWSs depends on complicated process control. Herein, we demonstrate parabola-shaped SWSs fabricated by simple process steps based on the combination of interference lithography, thermal reflow, and subsequent pattern transfer. A more detailed comparison and analysis between the cone and parabola shapes in terms of reflection characteristics is also made by using a rigorous coupled-wave analysis (RCWA) method.[31]

Figure 1 shows the contour plots of the reflectance variation as a function of wavelength for i) height and ii) incident angle in the SWSs with a) linear and b) paraboloid profiles. In the RCWA calculation, the period was fixed at 300 nm and the height was varied from 100 to 800 nm. GaAs was used as a substrate material, which is widely used in high-efficiency solar cells and other optoelectronic devices. The computational geometries of SWSs with cone and parabola shapes are shown in the insets of Figure 1a and b, respectively. As the height is increased, the reflectance tends to decrease and the low-reflectance region is broadened towards longer wavelengths. This could be explained by the fact that the effective refractive index is changed more slowly. For instance, cone arrays 600 nm in height provide a reflectance below 10% over a very wide wavelength range of 300–2800 nm, whereas it is limited only to the wavelength range of 300–1700 nm for arrays 300 nm in height. More interestingly, this antireflection range depends on the tapered profile of the SWSs as well as the height.

As shown in Figure 1b, the parabola-shaped SWSs with a height of 300 nm have a broader antireflection spectral range (i.e., 300–2200 nm) than that of the cone-shaped SWSs. This indicates that parabolic SWSs are more adequate for broadband antireflection than the conventional cone-shaped structures. To improve the light-absorption efficiency in photovoltaic devices (especially multijunction solar cells with a wide absorption band), an angle-independent broadband antireflection property is required. As depicted in plots (ii) of Figure 1a and b, the parabola-shaped SWSs reduce the reflectance much better over a wide spectral and angular range. The average reflectance of parabola-shaped SWSs is 19.03% in the wavelength range of 300–3000 nm and angular range of 0–90°, while that of cone-shaped SWSs is 22.26%.

[*] Prof. Y. T. Lee
Department of Nanobio Materials and Electronics
School of Photon Science and Technology
Gwangju Institute of Science and Technology
1 Oryong-dong, Buk-gu, Gwangju 500-712 (Korea)
E-mail: ytlee@gist.ac.kr

Prof. Y. T. Lee, Y. M. Song, S. J. Jang
Department of Information and Communication
Gwangju Institute of Science and Technology
1 Oryong-dong, Buk-gu, Gwangju 500-712 (Korea)

Prof. J. S. Yu
Department of Electronic and Radio Engineering
Kyung Hee University
1 Seocheon-dong, Giheung-gu,
Yongin-si, Gyeonggi-do 446-701 (Korea)

[**] This work was supported by the World Class University (WCU) program at GIST through a grant provided by MEST of Korea (R31-20008-000-10026-0).

DOI: 10.1002/smll.201000079

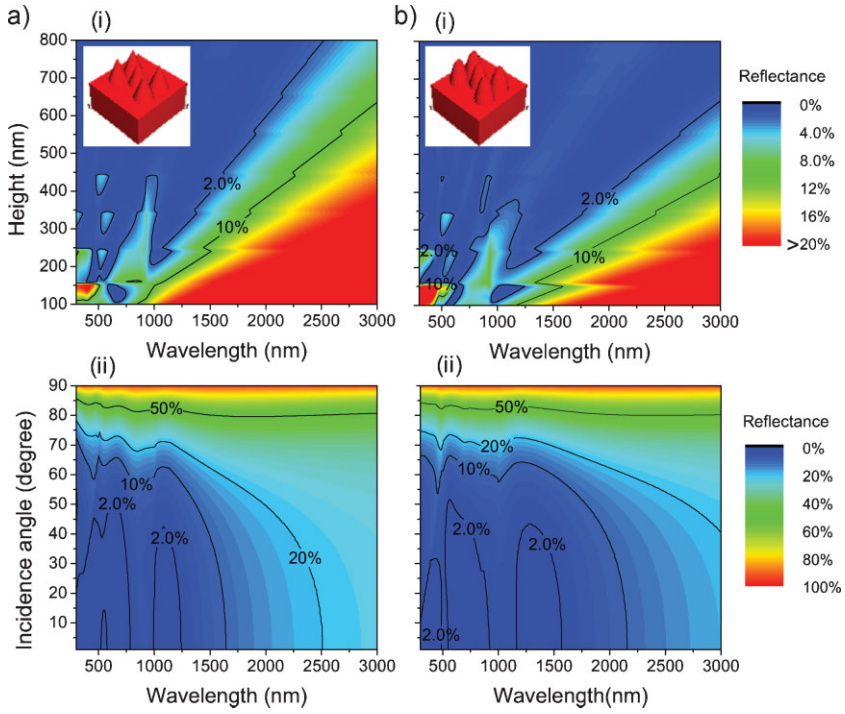

Figure 1. Contour plots of the reflectance variation as a function of wavelength for i) height and ii) incident angle in SWSs with a) linear and b) paraboloid profiles. The insets show the computational geometries of SWSs with cone and parabola shapes, respectively.

A schematic diagram of the fabrication procedure for parabola-shaped SWSs used in this experiment is shown in Figure 2. After the GaAs substrate is cleaned, it is spin-coated with diluted photoresist (PR). The dilution ratio and rotation speed are adjusted to obtain a 200-nm-thick resist layer. The PR is exposed, in two steps, to a laser interference pattern obtained with a 363.8 nm Ar laser. Between the two exposures, the substrate is rotated by 60°. After developing the patterns with a 300-nm period, a thermal reflow process is carried out on a hotplate to make lenslike PR shapes. More details about the thermal reflow process of the PR can be found in the literature.[13,32] After that, the PR-patterned GaAs substrate is etched by an inductively coupled plasma (ICP) etcher using a $SiCl_4$/Ar (2.5/60 sccm) gas mixture under a radio-frequency (RF) power of 100 W. To avoid isotropic etching at an inclined plane, a small portion of $SiCl_4$ gas is used. The scanning electron microscopy (SEM) images in Figure 2 show the pattern-transfer process caused by simultaneous etching of PR and GaAs as the etch time is increased. After complete etching of the lens-shaped PR, parabola-shaped SWSs with a smooth surface on the GaAs substrate are obtained.

Figure 3a–c shows SEM images of the parabola-shaped SWSs fabricated at the process pressures of 2, 20, and 50 mTorr, respectively. The fabricated SWSs consist of parabolic grating patterns, thus resulting in a linearly graded index profile. An increase in the process pressure improves the etch selectivity of GaAs to PR, which leads to a taller height as can be seen in Figure 3c. In this experiment, the etch selectivity is varied from 1 to 3 simply by increasing the process pressure from 2 to 50 mTorr. This means that the aspect ratio, that is, the height under the same period, can be controlled easily by adjusting the process pressure during the ICP etch procedure without the use of a complex gas mixture or additional process steps.[33] Furthermore, it is noted that the morphology of the etched surface through the lenslike PR mask is extremely smooth and

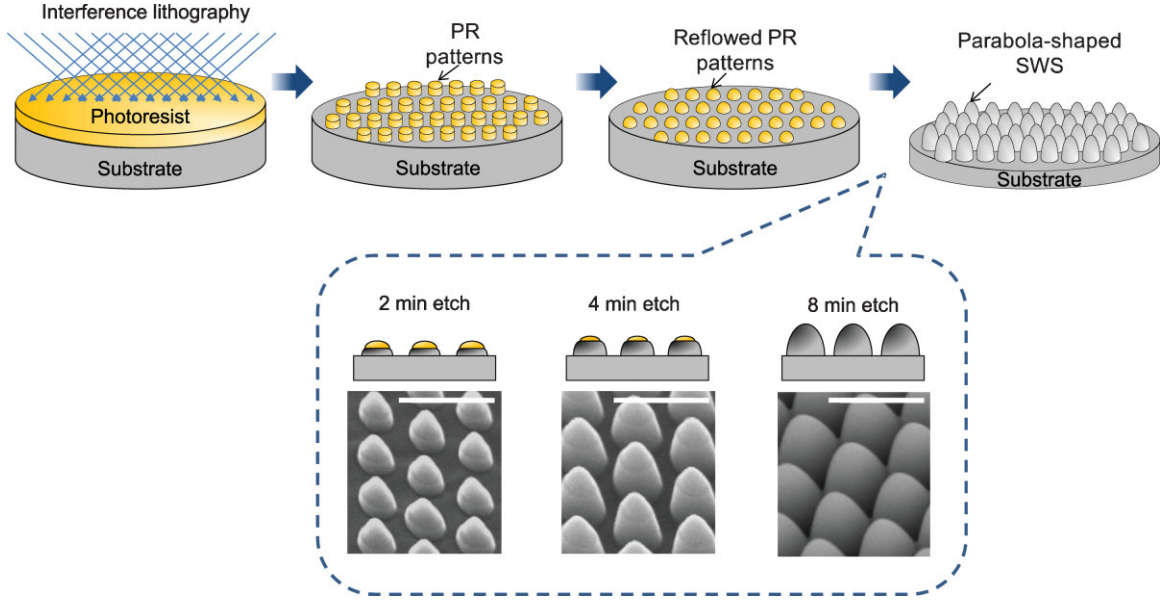

Figure 2. Schematic illustration of the fabrication procedure for parabola-shaped SWSs used in this experiment. Scale bar in SEM images: 500 nm.

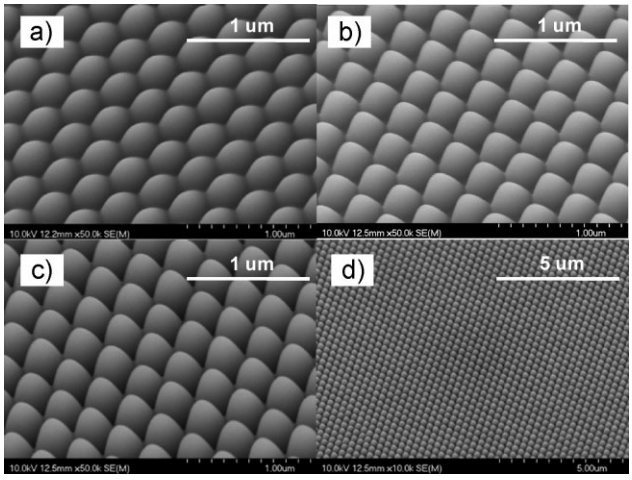

Figure 3. SEM images of the parabola-shaped SWSs fabricated at process pressures of a) 2, b) 20, and c) 50 mTorr. d) A lower-magnification image of (c).

these grating patterns are very uniform, as shown in the lower-magnification image (Figure 3d).

Figure 4 shows the measured reflectance as a function of wavelength for the fabricated parabola SWSs on a GaAs substrate at process pressures of 20 and 50 mTorr. The measured reflectance of bulk GaAs is also shown as a reference. Two SWS samples on the GaAs substrate suppress drastically the Fresnel reflection compared to that of a flat GaAs surface. As expected in Figure 1b, the parabola-shaped sample SWS2 fabricated at higher process pressure has a lower reflectance in the wavelength range of 300–2000 nm because of its taller height. The average reflectance of SWS2 is 7.80% in the wavelength range of 300–2000 nm, whereas that of parabola-shaped SWS1 is 11.05%.

To verify the effect of SWS shape on the reflection characteristics, cone-shaped SWSs were fabricated with the same period and height on a GaAs substrate. The fabrication processes of cone-shaped SWSs were essentially the same as those of parabola-shaped SWSs except for the dry-etch process condition by ICP. To induce the slight undercut at the sidewall,

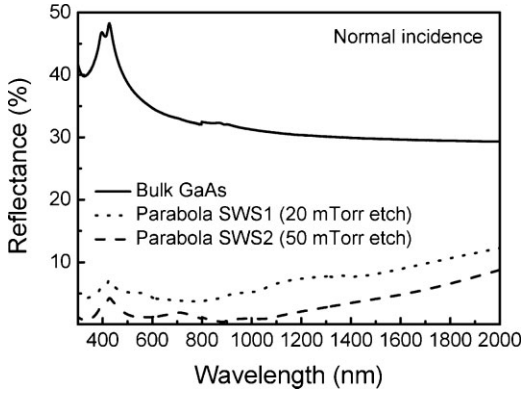

Figure 4. Measured reflectance as a function of wavelength for the fabricated parabola-shaped SWSs on a GaAs substrate at process pressures of 20 and 50 mTorr. The measured reflectance of bulk GaAs is shown as a reference.

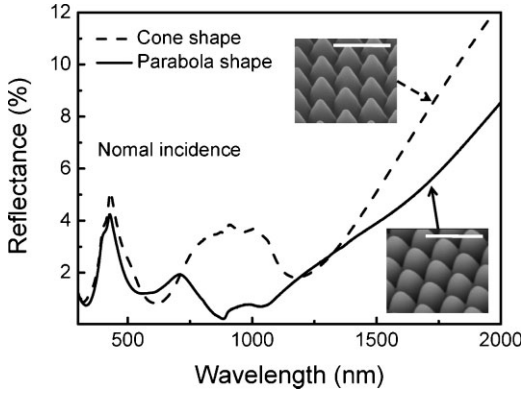

Figure 5. Measured reflectance spectra of the fabricated SWSs with cone (dashed line) and parabola (solid line) shapes. The insets show SEM images of the fabricated SWSs with cone and parabola shapes. Scale bar: 500 nm.

a larger amount of $SiCl_4$ gas (i.e., 7.5 sccm) was used compared to that of the etch process for parabola-shaped SWSs. The fabricated cone-shaped SWSs exhibit a linearly tapered profile, which provides a graded effective refractive index, as depicted in the upper inset of Figure 5. Unlike parabola-shaped SWSs, however, the effective index variation is more rapid at the bottom region of cone-shaped SWSs, which increase the Fresnel reflection at the graded area. Figure 5 shows measured reflectance spectra of the fabricated SWSs with cone and parabola shapes. The reflectance of cone- and parabola-shaped SWSs exhibits a similar tendency in the wavelength range below $\approx$700 nm, but above $\approx$700 nm the parabola-shaped SWSs exhibit a lower reflectance. It is clear that the reflection curve of cone-shaped SWSs is rapidly increased in the long-wavelength range. Therefore, the parabola-shaped SWSs allow low reflection to be achieved over a broader wavelength range.

In summary, we have demonstrated a simple technique for fabricating bioinspired antireflective parabola-shaped SWSs using a pattern-transfer process of rounded PR features. From the RCWA simulation and the experimental results, it is found that the SWSs with a parabola shape can significantly suppress the surface reflection in the longer-wavelength range compared to SWSs with a cone shape. This fabrication method for parabola-shaped SWSs with broadband antireflection characteristics has promising potential for various optoelectronic applications to improve device performance.

Experimental Section

Sample preparation: Semi-insulated, single-side polished GaAs (100) wafers (Wafer Technology Ltd., UK) were cleaned with acetone, methanol, and deionized water prior to the fabrication process. To remove native oxides, they were immersed in a concentrated HCl solution for 1 min, followed by a 3% NH_4OH solution for 30 s. To obtain a 200-nm-thick PR layer, AZ 5206-E (AZ Electronic Materials Ltd., USA) was diluted with AZ 1500 thinner. Exposure dose profiles of laser light were recorded on the resist using a laser-interference lithography system with a Lloyd's mirror and an argon laser ($\lambda = 363.8$ nm) as a light source. The

periodicity of the pattern was adjusted by controlling the incident angle of the laser. For an array of hexagonally arranged elliptical patterns, the substrate was rotated by 60°. The exposed resist was developed using AZ 300 MIF 2.38%. The thermal reflow process was carried out on a Shamal hotplate (HHP-411, Iuchi Seiei Dou Co., Japan) at 200°C for 40 s to make a lenslike PR shape. To transfer the pattern of lens-shaped PR to the GaAs substrate, a dry-etch process was conducted by using an ICP etcher (Plasmalab system 100, Oxford Instrument Co., UK). $SiCl_4$ and Ar were used as process gases, the RF power was 100 W, and the process temperature was 20 °C. The amount of $SiCl_4$ gas was varied from 2.5 to 7.5 sccm to modify the shape of the SWSs, and the process pressure was also changed from 2 to 50 mTorr to increase the height of the SWSs.

Characterization: The samples were characterized by field-emission SEM (S-4700, Hitachi, Japan) with an operating voltage of 10 kV. Reflectance spectra of the samples were measured by UV/Vis–near-IR spectrophotometry (Cary 5000, Varian, USA) in the wavelength range of 300–2000 nm.

Reflectance calculation: The RCWA method was used to calculate the reflectance of SWSs by using commercial software (DiffractMOD 3.1, RSoft Design Group, USA). In the RCWA calculation, cone- and parabola-shaped SWSs with sixfold hexagonal symmetry were modeled using linear and paraboloid tapered profiles in the radial direction. The dispersion of GaAs was considered to obtain the exact result at each wavelength.[34]

Keywords:
biomimetics · gallium arsenide · nanolithography · nanostructures · photovoltaic devices

[1] H. Sai, Y. Kanamori, K. Arafune, Y. Ohshita, M. Yamaguchi, *Prog. Photovoltaics* **2007**, *15*, 415–423.
[2] P. Yu, C.-H. Chang, C.-H. Chiu, C.-S. Yang, J.-C. Yu, H.-C. Kuo, S.-H. Hsu, Y.-C. Chang, *Adv. Mater.* **2009**, *21*, 1–4.
[3] Y. Kanamori, M. Ishimori, K. Hane, *IEEE Photonics Technol. Lett.* **2002**, *14*, 1064–1066.
[4] D.-S. Liu, T.-W. Lin, B.-W. Huang, F.-S. Juang, P.-H. Lei, C.-Z. Hu, *Appl. Phys. Lett.* **2009**, *94*, 143502.
[5] L.-C. Chen, C.-K. Wang, J.-B. Huang, L.-S. Hong, *Nanotechnology* **2009**, *20*, 085353.
[6] Y. M. Song, E. S. Choi, J. S. Yu, Y. T. Lee, *Opt. Express* **2009**, *17*, 20991–20997.
[7] C. Lee, S. Y. Bae, S. Mobasser, H. Manohara, *Nano Lett.* **2005**, *5*, 2438–2442.
[8] Y. Kanamori, H. Kikuta, K. Hane, *Jpn. J. Appl. Phys.* **2000**, *7B*, L735–L737.
[9] T. Lohmüller, M. Helgert, M. Sundermann, R. Brunner, J. P. Spatz, *Nano Lett.* **2008**, *8*, 1429–1433.
[10] P. Lalanne, G. M. Morris, *Nanotechnology* **1997**, *8*, 53–56.
[11] K. Hadobas, S. Kirsch, A. Carl, M. Acet, E. F. Wassermann, *Nanotechnology* **2000**, *11*, 161–164.
[12] X. Wang, Y. Liao, B. Liu, L. Ge, G. Li, S. Fu, Y. Chen, Z. Cui, *Microelectron. Eng.* **2008**, *85*, 910–913.
[13] Y. M. Song, S. Y. Bae, J. S. Yu, Y. T. Lee, *Opt. Lett.* **2009**, *34*, 1702–1704.
[14] S. A. Boden, D. M. Bagnall, *Appl. Phys. Lett.* **2008**, *93*, 133108.
[15] C.-H. Sun, W.-L. Min, N. C. Linn, P. Jiang, B. Jiang, *Appl. Phys. Lett.* **2007**, *91*, 231105.
[16] C. C. Striemer, P. M. Fauchet, *Appl. Phys. Lett.* **2002**, *81*, 2980–2982.
[17] G. Zhang, J. Zhang, G. Xie, Z. Liu, H. Shao, *Small* **2006**, *2*, 1440–1443.
[18] G. Xie, G. Zhang, F. Lin, J. Zhang, Z. Liu, S. Mu, *Nanotechnology* **2008**, *19*, 095605.
[19] W.-L. Min, P. Jiang, B. Jiang, *Nanotechnology* **2008**, *19*, 475604.
[20] C.-H. Sun, B. J. Ho, B. Jiang, P. Jiang, *Opt. Lett.* **2008**, *33*, 2224–2226.
[21] H. Xu, N. Lu, D. Qi, J. Hao, L. Gao, B. Zhang, L. Chi, *Small* **2008**, *4*, 1972–1975.
[22] S. Wang, X. Z. Yu, H. T. Fan, *Appl. Phys. Lett.* **2007**, *91*, 061105.
[23] Y. Kojima, T. Kato, *Nanotechnology* **2008**, *19*, 255605.
[24] S. L. Diedenhofen, G. Vecchi, R. E. Algra, A. Hartsuiker, O. L. Muskens, G. Immink, E. P. A. M. Bakkers, W. L. Vos, J. G. Rivas, *Adv. Mater.* **2009**, *21*, 973–978.
[25] C.-M. Hsu, S. T. Connor, M. X. Tang, Y. Cui, *Appl. Phys. Lett.* **2008**, *93*, 133109.
[26] J. Zhu, Z. Yu, G. F. Burkhard, C.-M. Hsu, S. T. Connor, Y. Xu, Q. Wang, M. McGehee, S. Fan, Y. Cui, *Nano Lett.* **2009**, *9*, 279–282.
[27] Y.-J. Lee, D. S. Ruby, D. W. Peters, B. B. McKenzie, J. W. P. Hsu, *Nano Lett.* **2008**, *8*, 1501–1505.
[28] Y.-F. Huang, S. Chattopadhyay, Y.-J. Jen, C.-Y. Peng, T.-A. Liu, Y.-K. Hsu, C.-L. Pan, H.-C. Lo, C.-S. Hsu, Y.-H. Chang, C.-S. Lee, K.-S. Chen, L.-C. Chen, *Nat. Nanotechnol.* **2007**, *2*, 770–774.
[29] Y. Li, J. Zhang, S. Zhu, H. Dong, Z. Wang, Z. Sun, J. Guo, B. Yang, *J. Mater. Chem.* **2009**, *19*, 1806–1810.
[30] D. G. Stavenga, S. Foletti, G. Palasantzas, K. Arikawa, *Proc. R. Soc. London Ser. B* **2006**, *273*, 661–667.
[31] M. G. Moharam, *Proc. SPIE* **1988**, *883*, 8–11.
[32] P. Nussbaum, R. Volkel, H. P. Herzig, M. Eisner, S. Haselbeck, *Pure Appl. Opt.* **1997**, *6*, 617–636.
[33] M. Karlsson, F. Nikolajeff, *Appl. Opt.* **2002**, *41*, 902–908.
[34] S. Zollner, *J. Appl. Phys.* **2001**, *90*, 515–517.

Received: January 19, 2010
Revised: March 12, 2010

